mary object, otherwise the resultant change in brightness will not be detectable. For example, although Pluto's eclipses are expected to be deep and narrow, they are detectable only during five or six apparitions around the time of passage of Earth through Pluto's orbital plane (*15*), that is, approximately 4 percent of the time. Even during these favorable apparitions, however, eclipse phenomena are occurring less than 7 percent of the time. It is no wonder then that, whereas we have known Pluto's rotation period for over 20 years (*16*), its rather large satellite has been discovered only recently and from images on photographic plates, and not through lightcurve observations. Herculina's satellite would have been similarly difficult to detect since a brightness drop of 0.10 magnitude may go unnoticed if the primary object is appreciably nonspherical. Nevertheless, now that we know what to look for, it may indeed be possible to detect eclipse events in asteroid lightcurves.

Examples of effects that may be attributable to eclipse events include the following: (i) the contact binarylike lightcurve of 44 Nysa (*17*), (ii) lightcurve maxima sharper than minima seen for 129 Antigone (*18*), (iii) the complex lightcurves seen for 29 Amphitrite (*19*) and 51 Nemausa (*20*), (iv) the lightcurve with triple maxima and minima observed for 1580 Betulia (*21*), (v) the increasing lightcurve amplitude with increasing solar phase angle seen for 349 Dembowska, 354 Eleanora (*22*), and 944 Hidalgo (*5*), and (vi) asteroids such as 532 Herculina (*20, 23*) whose lightcurves show two maxima and minima per cycle at one apparition but only one maximum and one minimum per cycle at another apparition.

Binzel and Van Flandern (*6*) note that binary systems are gravitationally stable for the lifetime of the solar system. Binary systems will be disrupted by collisions, however, on a shorter time scale; thus, few such systems would be primordial. Where do they come from then? I suggest that, whereas at least three of the 13 Themis family asteroids for which I obtained lightcurves show evidence of being binary (*3*), this being a larger proportion than is true of asteroids in general, and since the origin of at least each of the first three Hirayama dynamical families, of which the Themis family is one, from single parent bodies in catastrophic events is well established (*3, 24*), the evidence strongly suggests that the formation of binary asteroids is connected with these catastrophic events. These families are thought to be no more than half the age of the solar system (*25*), and perhaps much younger. Steins (*26*) suggested a lower limit on the age of the Eos family of only 1.5×10^6 years. The escape velocity from the surface of a 150-km spherical asteroid having a density of 3 g cm^{-3} is on the order of 100 m sec^{-1}, whereas the root-mean-square speed of the fragments at the time of disruption has been estimated by Williams (*27*) to be 270 m sec^{-1}. Thus the idea that binary asteroids formed in the relatively recent past during multibody interactions occurring immediately after the catastrophic event which produces an asteroid family is consistent with the known facts.

Binary asteroid pairs could be directly detected through additional occultation observations, space telescope imaging, or interferometric techniques. Additional lightcurve observations at a number of phase angles and at several different apparitions would allow the densities of these binary asteroids to be determined. These observations would provide valuable information, unavailable from any other presently known method, on the bulk properties of asteroids.

EDWARD F. TEDESCO
Lunar and Planetary Laboratory, University of Arizona, Tucson 85721

References and Notes

1. H. N. Russell, *Astrophys. J.* **24**, 1 (1906).
2. J. L. Dunlap and T. Gehrels, *Astron. J.* **74**, 796 (1969); J. Veverka, thesis, Harvard University (1970); W. Wamsteker and R. E. Sather, *Astron. J.* **79**, 1465 (1974); E. F. Tedesco, *Icarus* **28**, 21 (1976); J. Degewij, thesis, Leiden University (1978).
3. E. F. Tedesco, thesis, New Mexico State University (1979).
4. J. Degewij and B. Zellner, *Lunar Planet. Sci.* **9**, 235 (1978); J. Gradie, E. Tedesco, B. Zellner, *Bull. Am. Astron. Soc.* **10**, 595 (1978).
5. E. F. Tedesco, E. Bowell, B. Zellner, in preparation.
6. R. P. Binzel and T. C. Van Flandern, *Science* **203**, 903 (1979).
7. F. Scaltriti, V. Zappalà, H. J. Schober, *Astron. Astrophys. Suppl. Ser.*, in press.
8. D. Morrison, *Icarus* **31**, 185 (1977).
9. J. Schubart, *Astron. Astrophys.* **30**, 289 (1974).
10. H. R. Aggarwas and V. R. Oberdeck, *Astrophys. J.* **191**, 577 (1974); T. V. Johnson and T. R. McGetchin, *Icarus* **18**, 612 (1973).
11. J. H. McMahon, *Minor Planet Bull.* **6**, 14 (1978); D. W. Dunham, *Occultation Newsl.* **1** (No. 15), 151 (1978).
12. D. W. Dunham and P. D. Maley, *Occultation Newsl.* **1** (No. 11), 115 (1977); D. W. Dunham, *Bull. Am. Astron. Soc.* **9**, 621 (1978).
13. E. Bowell *et al.*, *Bull. Am. Astron. Soc.* **10**, 594 (1978). The distance of Herculina's satellite is such that it cannot be in synchronous orbit. A week after this report was submitted observations of the occultation of SAO 114159 by 18 Melpomene produced additional evidence, perhaps the best to date, of a secondary event, strongly implying that a satellite of Melpomene has been detected [B. G. Marsden, *Int. Astron. Union Circ. 3315* (1978)].
14. J. W. Christy and R. J. Harrington, *Astron. J.* **83**, 1005 (1978).
15. L. E. Anderson, *Bull. Am. Astron. Soc.* **10**, 586 (1978).
16. M. F. Walker and R. Hardie, *Publ. Astron. Soc. Pac.* **67**, 224 (1955).
17. I. Groeneveld and G. P. Kuiper, *Astrophys. J.* **120**, 529 (1954); A. V. Shatzel, *ibid.*, p. 547.
18. F. Scaltriti and V. Zappalà, *Astron. Astrophys.* **56**, 7 (1977).
19. H. Debehogne, A. Surdej, J. Surdej, *Astron. Astrophys. Suppl. Ser.* **32**, 127 (1978); I. van Houten-Groeneveld, C. J. van Houten, V. Zappalà, *ibid.*, in press.
20. Y. C. Chang and C. S. Chang, *Acta Astron. Sin.* **11**, 139 (1963); W. Wamsteker and R. E. Sather, *Astron. J.* **79**, 1465 (1974).
21. E. Tedesco, J. Drummond, M. Candy, P. Birch, I. Nikoloff, B. Zellner, *Icarus* **35**, 344 (1978).
22. V. Zappalà, I. van Houten-Groeneveld, C. J. van Houten, *Astron. Astrophys. Suppl. Ser.*, in press.
23. A. Harris and J. Young, *Icarus*, in press.
24. J. Gradie and B. Zellner, *Science* **197**, 254 (1977); J. Degewij, J. Gradie, B. Zellner, *Astron. J.* **83**, 643 (1978); J. Gradie, thesis, University of Arizona (1978).
25. E. Anders, *Icarus* **4**, 398 (1965).
26. K. A. Steins, *Astron. Zh.* **33**, 246 (1956).
27. J. G. Williams, *Bull. Am. Astron. Soc.* **7**, 343 (1975).

8 December 1978; revised 18 January 1979

Strain-Softening Instability Model for the San Fernando Earthquake

Abstract. *Changes in the ground elevation observed before and immediately after the 1971 San Fernando, California, earthquake are consistent with a theoretical model in which fault zone rocks are strain-softening after peak stress. The model implies that the slip rate of the fault increased to about 0.1 meter per year near the focus before the earthquake.*

Several precise theoretical models for earthquake instability and associated precursory deformation have recently been proposed. The models that postulate a strain-softening fault zone after peak stress either lack a stress-free ground surface (*1*) and thus are not easily compared with geodetic observations or are for long, vertical, strike-slip faults (*2, 3*) for which few observations have been made. Because the most complete, although still limited, observations for the time before and after an earthquake were those made for the 1971 San Fernando thrust event (*4, 5*), I have formulated a thrust fault version of an earlier strike-slip instability model. The agreement between theoretical and observed values of uplift and earthquake parameters implies that the slip rate of the fault increased near the focus before the earthquake. Aseismic fault slippage before the San Fernando earthquake has been postulated (*4, 6*).

Instability models may be useful for anticipating earthquakes. In theory, the

 0036-8075/79/0302-0907$00.50/0

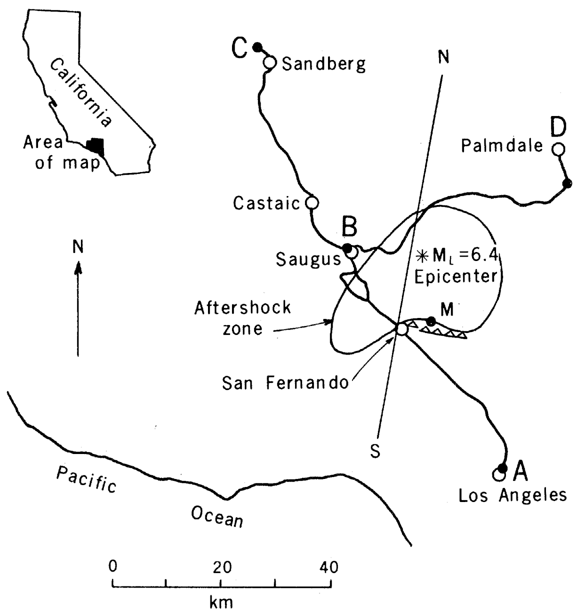

Fig. 1. Location of the San Fernando earthquake epicenter, the ground breakage (line with barbs on the upper plate), the approximate aftershock area, and survey line endpoints A, B, C, and D.

ground deformation rates near the fault change in time as the remotely applied displacement or stress increases. When the fault zone weakens during straining faster than the nearby elastic stress can decrease, an inertia-limited instability—an earthquake analog—occurs. In contrast, when the fault weakens slowly enough, a rapid but entirely quasi-static fault slip episode results. Because instability models admit both unstable and stable faulting modes according to the values of geometric and constitutive parameters used, mathematical inversion of the geodetic observations may make it possible to estimate the likelihood of earthquake instability.

Figure 1 shows the location of the epicenter of the San Fernando earthquake (local magnitude $M_L = 6.4$), the trace of coseismic ground surface breakage, the area of aftershock epicenters, and the resurveyed level lines AB, BC, and BD used here. Analyses of coseismic vertical and horizontal ground displacement changes based on the use of dislocation theory (*6–8*) and the finite element method (*9*) indicate that left-lateral thrust slippage occurred on fault planes of average dip between 30°N and 45°N and strike N10°E. The inferred average left-lateral and thrust components of slip are 1 to 2 m. The probable hypocenter depth is estimated to be 8.4 km, although a greater depth is not ruled out (*10*). The most recent study (*11*) gives a depth of 13 km. Whitcomb *et al.* (*10*) suggested that seismic slip occurred on the eastern segment of a fault surface that steps down several kilometers to the west. The entire projected fault surface coincides with the aftershock area in Fig. 1, and the nearly vertical downstep strikes N10°E coincident with the north-south line. The observed maximum slip at the ground rupture was about 1 m for the left-lateral and 1 m for the thrust components south of point M (*12*). The maximum coseismic uplift at point M was 2 m.

Level lines AB and BC were surveyed in 1964, 1965, 1968, and 1971 and tied to a nearly stationary benchmark south of Los Angeles (Tidal 8). Figure 2a shows the line elevation data for 1965, 1968, and 1971 with respect to the 1964 leveling; the uplift data are taken unaltered from figure 3 of (*5*). In 1968 and 1969, line CBD was also surveyed. The 1969 data for line BC (Fig. 2a) are tied to the 1964 datum on the basis of the assumption that the negligible uplift rate at point D of 0.005 m/year from 1965 to 1968 continued through 1969 [figure 2 of (*4*)]. The elevation errors of the lines after 1964 in Fig. 2a have a standard deviation of less than ± 0.02 m (*4*). I will compare the succession of observed pre- and post-earthquake uplift profiles (Fig. 2a) with a similar theoretical set from the two-dimensional instability model that has a 30° dipping fault plane. For the comparison, benchmark positions on line ABC are projected onto the north-south line normal to the fault trace. Because the level line ABC neither intersects the fault trace at the maximum offset nor passes through the maximum uplift, the model fault slip probably underestimates the actual fault slip by about five times.

In the model shown in Fig. 2b, the crust is represented by two homogeneous and Poisson elastic trapezoidal plates abutting at the fault plane. Boundary conditions simulating initially growing regional forces are a monotonically increasing horizontal displacement U applied at the end and bottom of the left plate. Vertical displacements are zero at the same two boundaries. The end and bottom of the right plate are fixed. The stress state depends solely on U and fault zone properties, which here are in the form of a slip- and depth-dependent friction law.

By assumption, the fault friction law

$$\tau(u, \zeta) = S \exp \left[- \left(\frac{u - u_0}{a} \right)^2 \right] \exp \left[- \left(\frac{\zeta - \zeta_0}{b} \right)^2 \right] \quad (1)$$

varies according to the Gaussian of fault slip u and downdip distance ζ; S is the greatest peak stress (obtained at $u = u_0$, $\zeta = \zeta_0$), u_0 is the slip at peak stress, a is the friction law width in slip, and b is the peak stress width on the fault plane. The first exponential term in Eq. 1 may be thought of as a bell-shaped, stress-strain law at a given depth; the second exponential term describes the variation of peak stress with depth. A similar law is used in instability models of strike-slip faults (*2, 3*).

This fault law is intended to approximate the brittle deformation component of a thin fault zone at low strain rate. A friction law form is used for mathematical convenience and does not imply a necessary connection with laboratory friction experiments. However, strain-softening after peak stress is observed in laboratory deformation of bulk samples (*1, 2*). In the laboratory the lower yield stress at large strain is nonzero, whereas stress in Eq. 1 vanishes at large slip. The residual stress may be considered part of the arbitrary stress field that may be added to model stresses induced by Eq. 1.

For the San Fernando earthquake, the origin is at the fault trace, the plate ends are at $x = +120, -55.5$ km, and the plate bottom is at $y = 37.5$ km. In addition, $\zeta_0 = 15$ km, $S\zeta_0/\mu = 1$ m, and $\Delta U/\Delta t = 0.045$ m/year, where μ is the plate rigidity and $\Delta U/\Delta t$ is the displacement rate of the remote boundary. These parameters are estimated by repeated attempts at matching the observed uplift and yield an acceptable visual fit to the uplift data. The consequences of varying model parameters are described below.

A sequence of fault loading and instability is simulated by repeatedly incrementing the boundary displacement U by ΔU. At each U the quasi-static displacement field in the plates is found by an iterative finite-element method such that the nonlinear friction law is satisfied (2). The fault plane is free to flex in the x-y plane, but fault friction is independent of changes in normal stress acting across the fault plane. Normal stress changes may be neglected because both shear and normal stress changes are of the order of S (10 to 100 bars), which is small compared to the confining pressure at focal depths. The 328 nearly equant triangular elements increase in width from about 1.5 km near ζ_0 to about 25 km at the plate ends. Instability occurs when $\partial \bar{u}/\partial U \rightarrow \infty$, where $\bar{u}$ is the average fault slip. At instability, an arbitrarily small increase of U causes a sudden jump of u to a new quasi-static solution which is taken to be an approximate analog of the postseismic state.

The theoretical and observed uplift profiles are compared in Fig. 2a. The three main theoretical results are as follows: (i) the position of maximum uplift before instability migrates leftward toward the fault trace with increasing time (increasing U), (ii) the uplift rate at the maximum increases, and (iii) the cumulative preinstability uplift change is about one-fifth of the uplift change near the fault trace during instability. Physically, the horizontal migration and increasing rate of the uplift is caused by a rapid pile-up and updip migration of edge dislocations generated during slip-softening immediately below the position ζ_0.

Agreement between theory and observation is reasonably good for all level lines except the postseismic line 1971. The theoretical uplift overestimates the observed 1971 uplift in the epicentral area. Postinstability fault stress in this case is everywhere $\tau/S = 0.2$. When Eq. 1 is used to obtain the postinstability state, fault friction is essentially zero, the maximum ground surface uplift is 1.07 m at the trace, and the unstable slippage at large ζ is unrealistically large. The rationale for temporarily higher postinstability friction stress is that Eq. 1 is most appropriate for low strain rates long before instability, but a viscous stress should be added during high strain rates just before and during instability. Even with the viscous stress approximation, the postearthquake elevation near the epicenter is much greater than observed. The cause is unknown but might be inhomogeneity or nonlinear and nonelastic deformation in the crust or coseismic normal faulting on the San Gabriel fault 7 km north of the San Fernando trace (7).

In the model, the fault slip rate and acceleration are greatest slightly below $\zeta_0 = 15$ km just prior to instability. Neglecting possible viscous effects, this position is probably a good estimate of the earthquake focus because inertial forces would first become important here. Langston (11) estimated the epicenter to be 15 km from the fault trace (Fig. 2b) and the hypocenter to be 13 km deep. This epicenter projects downward to $\zeta = 17$ km and $y = 9$ km. At the onset of unstable slippage, most of the fault has weakened and frictional stresses are near the peak stress only close to ζ_0.

Figure 2c shows the theoretical fault slip taking place during successive time intervals. The position of the greatest fault slip rate moves updip and increases before instability. Fault slip during instability decreases with depth more rapidly when the postinstability friction is $\tau/S = 0.2$ than when Eq. 1 is used. The

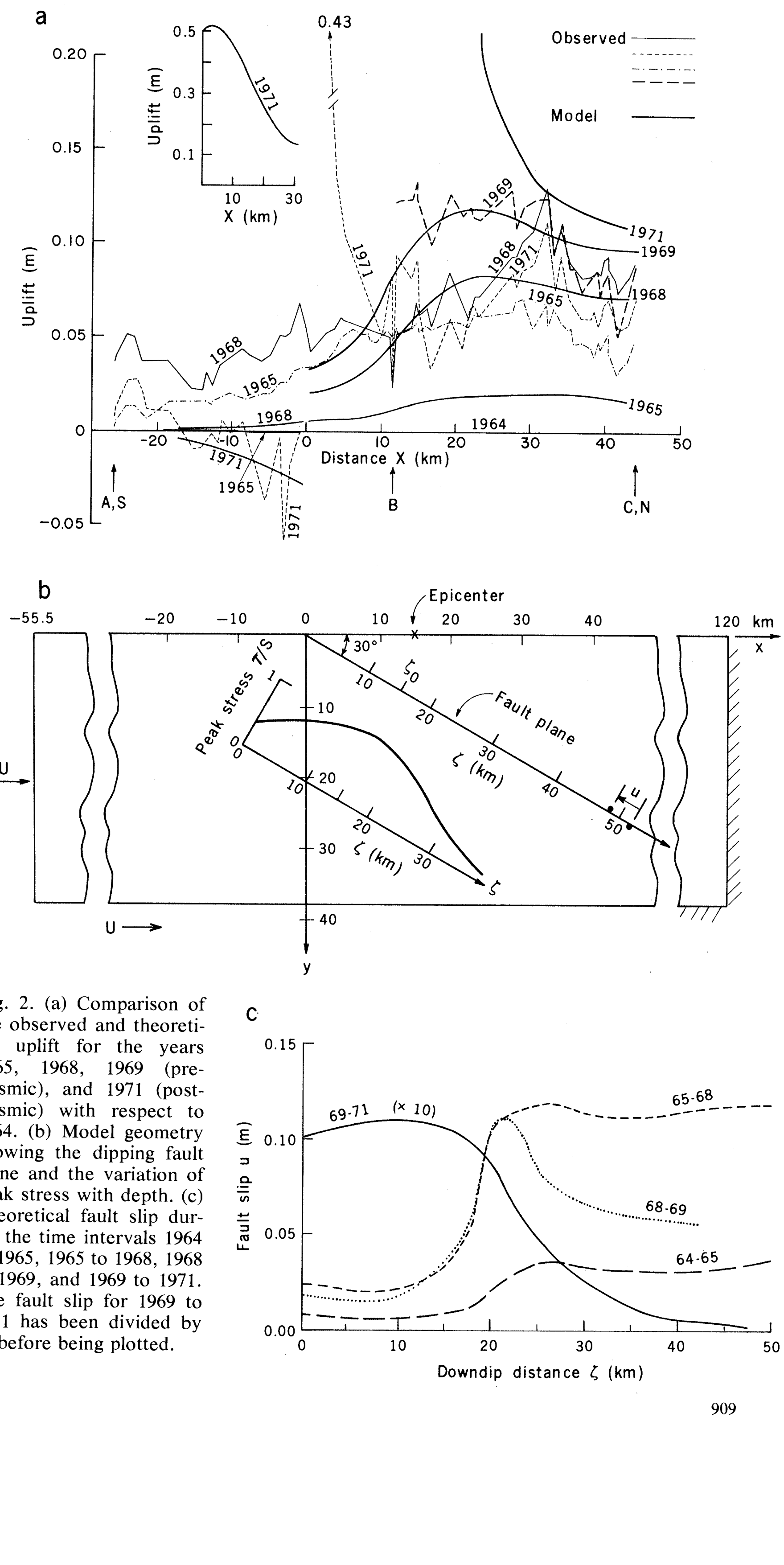

Fig. 2. (a) Comparison of the observed and theoretical uplift for the years 1965, 1968, 1969 (preseismic), and 1971 (postseismic) with respect to 1964. (b) Model geometry showing the dipping fault plane and the variation of peak stress with depth. (c) Theoretical fault slip during the time intervals 1964 to 1965, 1965 to 1968, 1968 to 1969, and 1969 to 1971. The fault slip for 1969 to 1971 has been divided by 10 before being plotted.

unstable slip reaches a maximum near $\zeta = 10$. Other investigators (7, 9) have inferred that fault slip reaches a maximum of 4 to 8 m at $\zeta = 2$ km before declining toward the surface.

A similar updip migration of fault slip has been inferred by Thatcher (6) who modeled fault slip with edge dislocations. That model predicts increasing preseismic subsidence south of the fault trace unless a decreasing fault dip with depth is also proposed. Several other studies favor an increasing dip with depth (7, 9-11). By comparison, the instability model uplift agrees in sign with the observed preseismic uplift south of the fault trace. In addition, such dislocation models impose the amount and distribution of fault slip at constant remote (boundary condition) stress, whereas fault slip in the instability model is part of the solution and remote stresses increase and then decrease prior to instability.

Scaling the friction law, Hooke's law, and the equilibrium equations by a representative length ζ_0, stress S, and displacement a shows that mechanically similar solutions are characterized by two dimensionless variables $\mu' = \mu a/S\zeta_0$ and $b' = b/\zeta_0$ for fixed plate geometry and fault dip. Thus doubling μ has the same effect on stability as halving S. The results (Fig. 2) correspond to $\mu' = 0.3$, $b' = 1$. As in the strike-slip fault models (2, 3), increasing μ' or decreasing b' causes unstable deformation to be replaced by temporarily rapid quasi-static deformation. The boundary between unstable and stable deformation is near $\mu' = 2$ for $b' = 1$.

Uplift profiles for stable cases differ from those for unstable cases by being broader in space and showing more gradual changes with increasing U. The origin of the differences is readily seen in view of the fact that increasing $\mu' = \mu a/S\zeta_0$ inhibits instability. For example, μ' might be increased by a higher μ. A less flexible crust will tend to smooth deformation gradients.

I made additional simulations to determine the effect of varying the dip, μ', and b' in turn. In all the simulations, I used dimensionless variables and chose values of ζ_0 and $S\zeta_0/\mu$ to match the amplitude and position of the observed 1969 profile. Increasing the dip to 40° makes the epicentral uplift profiles slightly more peaked but increases by about 50 percent the uplift jump at the fault trace. Setting $\mu' = 1$ increases the uplift jump at the fault two to three times, but unstable uplift is about one-half that for $\mu = 0.3$. With $b' = 2$, the overall fit is slightly better than with $b' = 1$, but ζ_0 must be increased to 20 km, giving a distance from the fault trace to the epicenter of 16 km. For fixed dip, μ', and b', halving $\Delta U/\Delta t$ decreases the 1965 and 1968 uplifts by about 1 cm. The quantity $\Delta U/\Delta t$ is poorly constrained by field observations.

The changes in elevation shown in Fig. 2a are part of the much broader (~ 150 km wide) Palmdale uplift, which started in 1960 (13). The Palmdale uplift is qualitatively consistent with uplift expected from slip-softening on a northeast-dipping thrust fault of comparable space scale, part of which may have slipped to cause the San Fernando earthquake. The temporarily rapid but aseismic Palmdale uplift episodes may correspond to inertially stable deformation modes; the San Fernando earthquake would correspond to a smaller-scale unstable mode.

If the instability model assumptions are generally valid, one should expect accelerating precursory fault slip, mainly near the earthquake focus. Enhanced fault slip rates may be large enough to produce observable deformation changes at the free surface in the vicinity of the epicenter and ground breakage at the fault trace. Because gound deformation is theoretically different between unstable and stable models, an examination of the observations may make it possible to estimate the probability of earthquake instability. However, too few observations have been made thus far to permit such an attempt.

W. D. STUART

U.S. Geological Survey,
Menlo Park, California 94025

References and Notes

1. J. W. Rudnicki, *J. Geophys. Res.* **82**, 844 (1977); J. R. Rice, *Gerlands Beitr. Geophys.*, in press; ——— and J. W. Rudnicki, *J. Geophys. Res.*, in press.
2. W. D. Stuart, *J. Geophys. Res.*, in press.
3. ——— and G. M. Mavko, *ibid.*, in press.
4. R. O. Castle, J. N. Alt, J. C. Savage, E. I. Balazs, *Geology* **2**, 61 (1974).
5. R. O. Castle, J. P. Church, M. R. Elliott, N. L. Morrison, *Tectonophysics* **29**, 127 (1975).
6. W. Thatcher, *Science* **194**, 691 (1976).
7. R. W. Alewine and T. J. Jordan, *Geophys. J. R. Astron. Soc.* **35**, 357 (1973); R. W. Alewine, thesis, California Institute of Technology (1973).
8. J. C. Savage, R. O. Burford, W. T. Kinoshita, *Calif. Div. Mines Geol. Bull.* **196**, 175 (1975).
9. P. H. Jungels and G. A. Frazier, *J. Geophys. Res.* **78**, 5062 (1973).
10. J. H. Whitcomb, C. R. Allen, J. D. Garmany, J. A. Hileman, *Rev. Geophys. Space Phys.* **11**, 693 (1973).
11. C. A. Langston, *Bull. Seismol. Soc. Am.* **68**, 1 (1978).
12. B. Kamb, L. T. Silver, M. J. Abrams, B. A. Carter, T. H. Jordan, J. B. Minster, *U.S. Geol. Surv. Prof. Pap. 733* (1971), p. 41; *ibid.*, p. 55.
13. R. O. Castle, J. P. Church, M. R. Elliott, *Science* **192**, 251 (1976).
14. I thank R. O. Castle and W. Thatcher for comments.

15 August 1978; revised 30 October 1978

Protein Deficiency and Tribal Warfare in Amazonia: New Data

Abstract. *Increasing numbers of anthropological studies about native Amazonian warfare and demographic practices attempt to explain these phenomena as competition over or a response to scarce game animals and other sources of high-quality protein. Recently completed field research among the Yąnomamö Indians living at the Venezuela-Brazil border indicates that their protein intake is comparable to that found in highly developed industrialized nations and as much as 200 percent more than many nutritional authorities recommend as daily allowances. Recent data on other Amazonian tribes likewise fails to indicate a correlation between protein intake and intensity of warfare patterns.*

This report summarizes recently collected data on protein consumption among the Yąnomamö, a tribe of Tropical Forest Indians living at the Venezuelan-Brazilian border. While the data contribute to a more complete understanding of the nutritional status of the Yąnomamö, who have been the subject of extensive biomedical studies (1), our main objective is directed toward the growing tendency evident among exponents of cultural ecological theories to assume that Tropical Forest Indians subsist on a substandard diet that is deficient in high-quality protein. The Yąnomamö Indians constitute an important example of the possible relationship between protein consumption, warfare, and demographic practices such as infanticide and male-female dominance relationships. We have previously expressed our doubt that a protein shortage exists and have questioned the arguments that a protein shortage could adequately explain the complex relationships between demographic patterns, warfare, and social organization in this society (2, 3).

In a historical sense, the current anthropological interest in protein consumption among Amazonian tribes represents a specific component in the more general tendency for U.S. anthropologists to attempt to explain cultural forms of Amazonia by invoking environmental or ecological factors that are alleged to limit population growth, community size, and cultural complexity. Since the 1950's, a prevailing explanatory theme held that the deficient nature of the tropical forest soil accounted for the im-